Journal of Magnetism and Magnetic Materials 523 (2021) 167599

Contents lists available at ScienceDirect

Journal of Magnetism and Magnetic Materials

journal homepage: www.elsevier.com/locate/jmmm

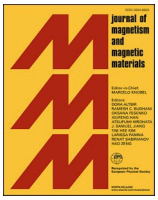

Geometric effects in cylindrical core/shell hard–soft exchange-coupled magnetic nanostructures

Namkyu Kim, Hee-Sung Han, Sooseok Lee, Min-Ji Kim, Dae-Han Jung, Myeonghawn Kang, Hyejin Ok, Youngkyun Son, Sukbin Lee *, Ki-Suk Lee *

School of Materials Science and Engineering, Ulsan National Institute of Science and Technology (UNIST), Ulsan 44919, Republic of Korea

ARTICLE INFO

Keywords:
Permanent magnet
Exchange spring magnet
Nanostructure
Energy product
Micromagnetic simulation

ABSTRACT

We explore the optimal condition for cylindrical core/shell hard-soft exchange-coupled magnetic nanostructures by obtaining full hysteresis loops for various geometries by obtaining full hysteresis loops for various geometrical variables, including the dimensional scale and soft/hard-magnetic phase volume ratio through micromagnetic simulations. For achieving maximum energy product (*BH*), it is essential to increase the demagnetizing field by increasing the volume fraction of the soft magnet while maintaining a positive nucleation field and, which can be possible by the scaling-down. To scale up the nanostructure to a bulk magnet having high *BH* can be achieved by forming an array of needle-shaped exchange-coupled cylinders. These findings could lead to the flexible design and scalable fabrication of exchange-coupled permanent magnets.

1. Introduction

Devices such as electric vehicles and wind power generators utilize the magnetic energy of permanent magnets [1,2]. To meet the increasing demand for such devices, researchers have actively developed permanent magnets with higher efficiencies and lower cost. Exchange-coupled magnets are prominent candidates because they can exploit the advantages of both soft and hard-magnetic materials [3–6]. They also require a lesser amount of expensive rare earth elements. These magnets can attain high magnetic energies owing to the exchange coupling between the high-anisotropy hard-magnetic phase and the high-saturation-magnetization soft-magnetic phase.

Magnetic energy is represented by the energy product *BH*, which is twice the energy stored in the stray field outside the magnet. It can be obtained from the volume integral of the square of the stray field outside the magnet, or from the volume integral of the dot product between the demagnetizing field $\boldsymbol{H}_{\mathrm{d}}$ and the internal magnetic flux density $\boldsymbol{B}$. The maximum energy product, $(BH)_{\max}$, is widely used as a figure of merit for evaluating the performance of hard-magnetic materials. As noted by Skomski and Coey *et al.* [7–9], $(BH)_{\max}$ should be evaluated rigorously from the hysteresis loop by considering the exact working point, which is determined by the shape of the magnet. Particularly for semi-hard magnets such as Alnico [10,11] and exchange-coupled magnets [7,8,12–14], the hysteresis loop varies significantly with the shape of the magnet. Thus, $(BH)_{\max}$ cannot be estimated from the hysteresis loop of a magnet with a specific shape, such as a thin film or powder; rather, it should be obtained from the *BH* values at the remanent state for magnets with various shapes [15–20].

In exchange-coupled magnets, the shape of the magnet has a great influence on the *BH* because not only the demagnetizing factor changes but also the area of the interphase between soft and hard phase for exchange-coupling. There is a trade-off with exchange hardening which maintains high remanent magnetization (M_{r}) by overcoming the shape anisotropy of the optimal shape through the interfacial exchange-coupling with hard phase. Recently, various studies have been actively carried out to find the optimal shape of the exchange-coupled magnet including layer-by-layer [7,21–23], core/shell structure [13,19,20,24–26], and mixed phase[12]. Since the layer-by-layer structure has the advantage of high packing efficiency, but it has a low nucleation field owing to strong demagnetizing field and nucleation mode by the layered structure, many researchers have been focused on controlling nucleation by manipulating the interlayer exchange coupling or thickness of the soft phase [21–22]. To obtain a high nucleation field through a large interface between soft and hard phase, the core/shell structure has been proposed [19,20,25]. Very recently, cylindrical core/shell microstructure [13,20,24,26] has been presented not only for high energy product value but also for high nucleation field. Despite such intensive theoretical and experimental works, the optimal

* Corresponding authors.
E-mail addresses: sukbinlee@unist.ac.kr (S. Lee), kisuk@unist.ac.kr (K.-S. Lee).

https://doi.org/10.1016/j.jmmm.2020.167599
Received 23 September 2020; Received in revised form 18 November 2020; Accepted 23 November 2020
Available online 5 December 2020

condition for maximizing energy product based on the precise evaluation of the *BH* values at the remanent state for exchange-coupled magnets with various shapes has been studied very rarely.

In this study, we performed micromagnetic simulations on core/shell hard–soft exchange-coupled magnetic cylinder with various geometrical parameters and wide-ranging volume ratios of the hard-to-soft phase, and rigorously evaluated the *BH* values at a working point considering the demagnetizing field, which is determined by shape. We explored the optimal geometry for maximizing *BH* by first examining the effects of dimensional scaling and phase ratio on a single exchange-coupled cylinder. Then, we examined the effects of scaling and the aspect ratio of the shape on arrays of exchange-coupled cylinders, with consideration of the shape of the array structure.

2. Simulation method

The exchange-coupled magnet model is illustrated in Fig. 1. We adopted a cylindrical core/shell nanostructure with length L, consisting of a hard-magnetic core with diameter D surrounded by a soft-magnetic shell of thickness t. We calculated the full hysteresis loop of the model using the finite differential micromagnetic solver MuMax^3[27]. We selected Sm_2Co_{17} as the hard-magnetic phase with an exchange stiffness $A_{ex,hard}$ of 1.4×10^{-11} J/m and saturation magnetization $M_{s,hard}$ of 1.034 MA/m^3. For the soft-magnetic phase, we selected FeCo with an exchange stiffness $A_{ex,soft}$ of 1.0×10^{-11} J/m and saturation magnetization $M_{s,soft}$ of 1.913 MA/m^3 [28–30]. In the finite differential calculation of the micromagnetic properties, a cubic cell of $2 \times 2 \times 2$ nm^3 was chosen, which was smaller than the exchange length of both phases. We assumed that the z-axis was the easy axis of magnetization of the hard-phase with a magnetocrystalline anisotropy constant of 3.3×10^6 J/m^3, whereas the soft-phase shell exhibited no crystalline anisotropy. We assumed perfect exchange coupling between the hard and soft phases with a harmonic mean value of A_{ex}/M_s for each phase [27]. To obtain full hysteresis loops, an external magnetic field ranging from −10 to +10 T was applied along the easy axis. To obtain the correct *BH* values, we calculated mean value of the dot product of $\boldsymbol{H}$ and $\boldsymbol{B}$ in each cell.

To investigate the effect of the volume fraction of the high-magnetization soft phase on *BH*, we calculated the full hysteresis loops of the hard–soft core/shell cylinder with various shell thicknesses, t. To maximize the internal field $\boldsymbol{H}_d$ at remanence, we assumed that the hard core had dimensions of $D = 48$ nm and $L = 24$ nm.

3. Results

As depicted in Fig. 2(a), the saturation magnetization M_s increases in proportion to the volume fraction of the high-magnetization soft-phase, f_s, according to the equation $M_s = (1 - f_s)M_{s,hard} + f_s M_{s,soft}$. However, the remanent magnetization M_r decreases suddenly when f_s exceeds 0.33 ($t = 6$ nm). As a result, *BH* also falls abruptly. Because the soft phase exhibits no crystalline anisotropy, its magnetization switching depends on the balance between shape anisotropy and exchange hardening. Exchange hardening is inversely proportional to t; therefore, when the volume of the soft-magnetic phase is increased by increasing t, the shape anisotropy becomes more dominant than exchange hardening. Consequently, when t exceeds a critical value, the soft-magnetic phase does not follow the axis of the hard-magnetic phase owing to its shape anisotropy. For our model system, the critical value is 4 nm and thus hysteresis loops for $t > 4$ nm in Fig. 2(a) show two nucleation fields, which reveals that the soft phase starts to switch first followed by the hard phase. Hence, the negative nucleation field H_N of the soft-magnetic phase in the hysteresis loop can cause a sudden reduction in M_r.

Fig. 2(b) illustrates the second quadrant of the *B–H* loops (left-hand side, LHS) and the energy product *BH* (right-hand side, RHS) for core/shell magnets with different volume fractions of the soft-magnetic phase. The lines and symbols on the RHS represent the *BH* values and the working points at the remanent state for each geometry, respectively. To obtain the precise *BH* values, we integrated $\boldsymbol{B}\cdot\boldsymbol{H}$ in each cell for the whole volume instead of the conventional estimation derived from the area in the second quadrant of the *B–H* loop. There is a clear difference between *BH* calculated in two different ways. For instance, the integrated *BH* at the working point for $(D, t, L) = (48, 30, 24)$ as seen a green symbol in the RHS of Fig. 2(b) has nonzero value notwithstanding almost zero value of the area in the LHS of Fig. 2(b).

To estimate the effect of dimensional scaling on *BH*, we compared the hysteresis loops and *BH* values for various scales while maintaining $t = D/4$ and $L/D = 0.5$ (Fig. 2(c) and 2(d)). As the scale decreased, H_N moved in the positive direction. When D was reduced to 16 nm, H_N became positive, significantly increasing *BH* to 0.6934 MJ/m^3—twice the value for the hard-magnetic cylinder. This reveals that scaling has a significant effect on the balance between exchange hardening and shape anisotropy. Because shape anisotropy mainly depends on the aspect ratio of the shape, scaling down increases the dominance of exchange hardening. When reducing the scale of the magnet, the thickness of the soft-magnetic phase decreases proportionally to the scaling factor, whereas the soft-phase volume fraction (which determines the saturation magnetization) remains unchanged. As exchange hardening is inversely proportional to the thickness, it increases significantly in comparison with the shape anisotropy. Below a specific scale ($D = 16$ in Fig. 2(c)), H_N becomes positive, which considerably increases M_r and enables *BH* to reach its maximum value.

The scaling effect can be clearly observed in the plots of *BH* vs. f_s in Fig. 3(a) for various values of D. At small values of f_s, the *BH* plots follows the theoretical increment of $(BH)_{max}$ (dashed line) because of the enhancement of the saturation magnetization according to the equation

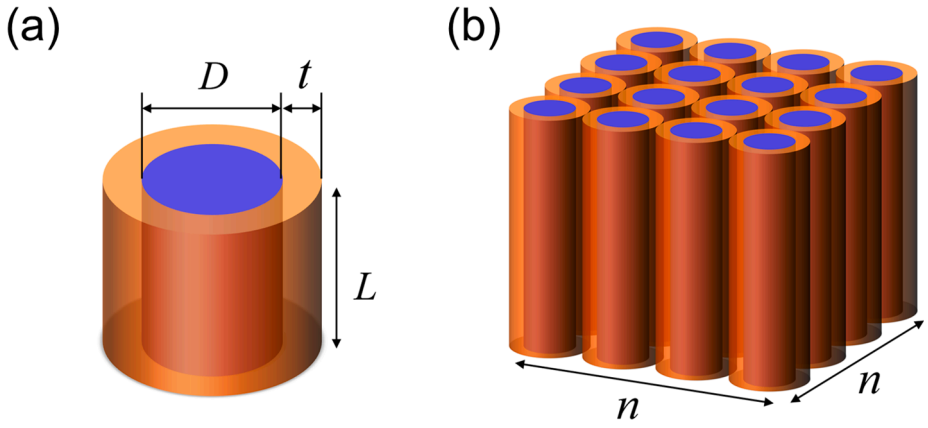

Fig. 1. (a) Schematic of cylindrical core/shell structure with length L composed of hard-magnetic core with diameter D and soft-magnetic shell with thickness t. (b) Schematic of $n \times n$ array of cylindrical core/shell structures with 2 nm intervals between the cylinders.

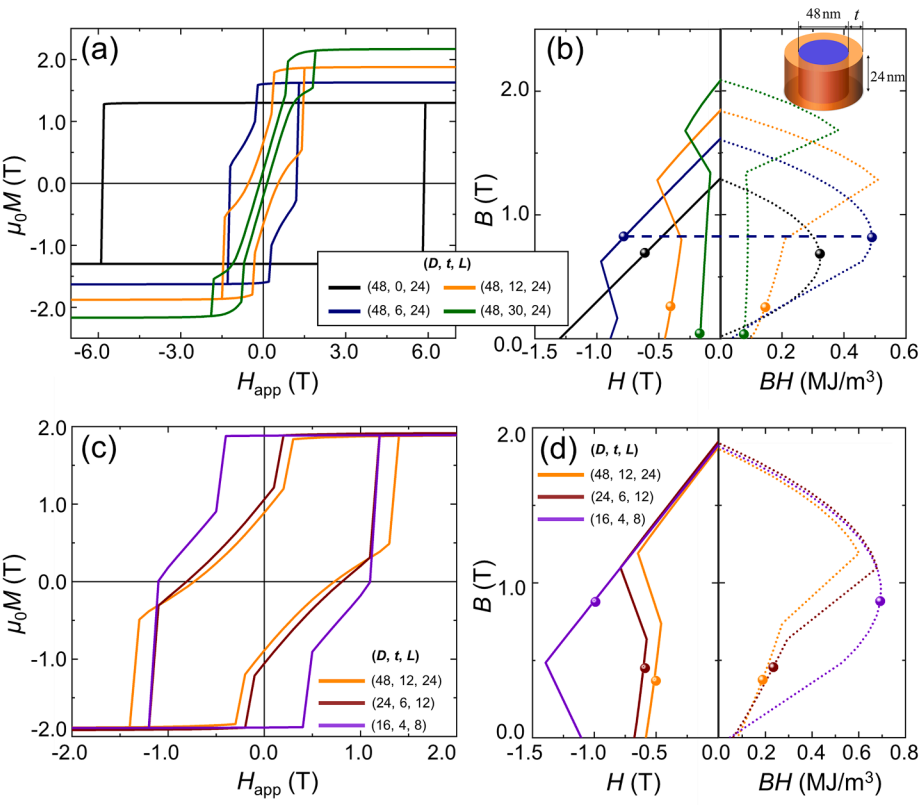

Fig. 2. (a) Hysteresis loops of magnetization $\mu_0 M$ by applied magnetic field H_{app} for different thickness (t) soft-magnetic shells. (b) Second quadrant of the B versus $H = H_{app} + H_d$ loop (left) and energy product BH (right) of cylindrical core/shell structure. The spherical markers indicate the magnetic flux considering the demagnetization field H_d when $H_{app} = 0$. The dotted lines on the right side of the graph are not meaningful, except the working points. (c) $\mu_0 M$–H_{app} hysteresis loop of cylindrical core/shell structures with different scales. (d) Second quadrant of the B–H loop (left) and energy product BH (right) of cylindrical core/shell structures. The spherical markers indicate the magnetic flux considering the demagnetization field when the external field is zero.

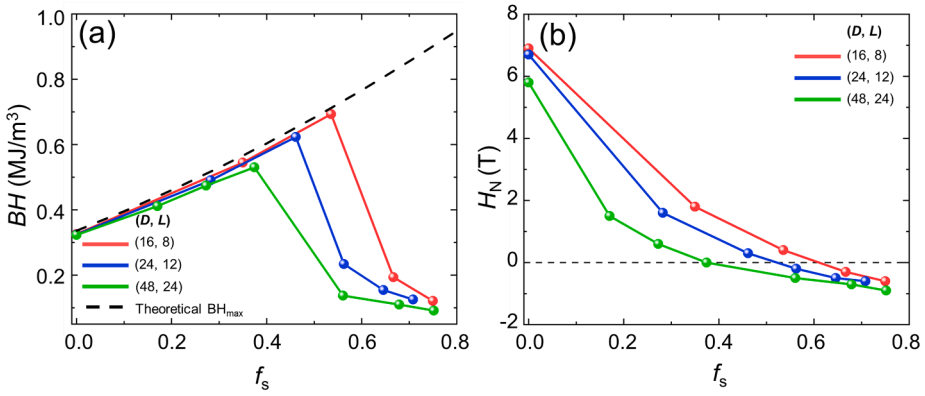

Fig. 3. (a) Energy product BH as a function of the soft-phase volume fraction f_s at different scales. The dashed black line represents the theoretical $(BH)_{max}$ according to f_s. (b) Nucleation field H_N of cylindrical core/shell structures as a function of f_s at different scales.

$(BH)_{max} = 1/2\mu_0(M_s)^2$. However, as f_s increases above a critical value, BH suddenly decreases. The f_s value at which the plot deviates from the theoretical estimation depends on the scale of the magnet; the larger the scale, the lower the critical value of f_s. Fig. 3(b) depicts the plots of H_N vs. f_s, in which the critical f_s value is directly related to the sign of the nucleation field. This indicates that it is crucial to maximize the soft-magnetic phase fraction as much as possible while keeping H_N positive. Consequently, a smaller-scale system that follows the theoretical $(BH)_{max}$ estimation up to a higher soft-phase fraction can result in a higher BH.

As mentioned in the previous paragraph, we demonstrated that a positive nucleation field is essential for achieving a viable exchange-coupled nanostructure magnet with a high BH. Moreover, a positive H_N can be attained by scaling down the size of the magnet. Nevertheless, scaling down may limit the design flexibility or feasibility of scalable fabrication. To address this problem, we considered an array of nanostructured exchange-coupled magnets, similar to Alnico magnets or packed structures [10,26,31,32]. The array structure enables the magnet to be scaled up while maintaining the dominance of exchange hardening within each element. In this manner, by varying the aspect ratio of the elements, the shape anisotropy may assist exchange hardening.

First, we explored the effect of the aspect ratio (L/D) of a single exchange-coupled nanostructure magnet. When $L/D < 1.0$, the easy axis by exchange hardening is perpendicular to that of shape anisotropy; hence, there is competition between them. However, as L increases, the easy axis of shape anisotropy aligns with that of exchange hardening, which enables the soft-magnetic phase to fully couple with the hard-magnetic phase, resulting in the hysteresis loops illustrated in Fig. 4 (a) and 4(b). In particular, for the case of $D = 24$ in Fig. 4(b), the negative H_N value becomes positive as L increases. Fig. 4(c) depicts the variation in H_N with the aspect ratio L/D at different scales. All plots demonstrate a similar trend with the shape-anisotropy energy for an

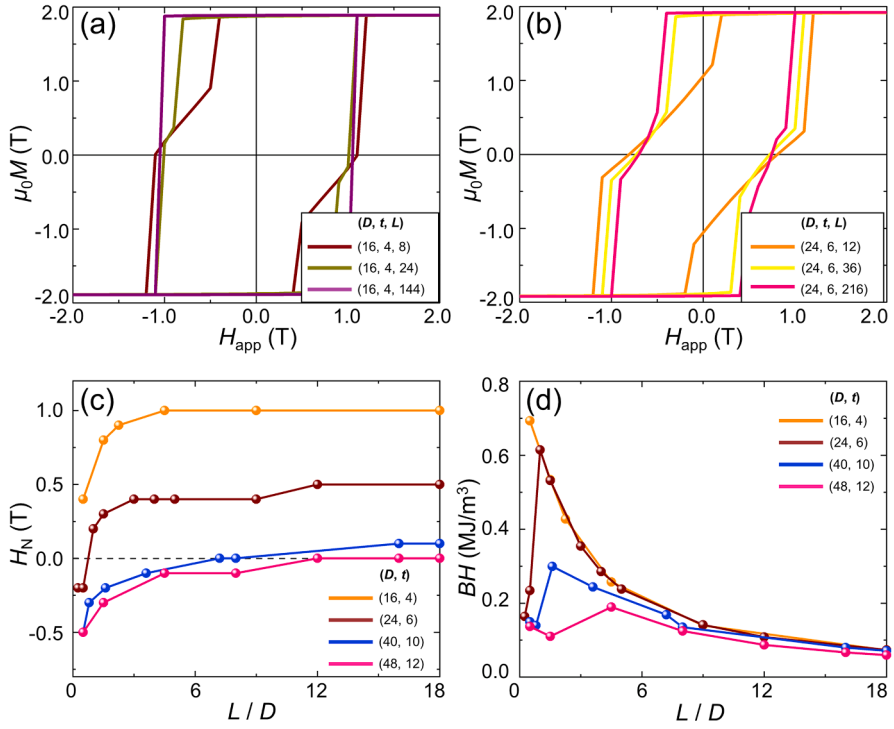

Fig. 4. μ_0M–H_{app} hysteresis loops of magnetization for magnets with (a) (D, t) = (16, 4) and (b) (D, t) = (24, 6) for different lengths (L). (c) Nucleation field H_N and (d) energy product BH of cylindrical core/shell structures as a function of the aspect ratio (L/D).

ellipsoid or cylinder [33], but with different offsets depending on the scaling. This is because exchange hardening depends on the scaling, whereas shape anisotropy does not. Interestingly, when $D = 48$ nm, H_N does not become positive even at significantly high values of L/D, although it is expected to be positive based on the coupling of shape anisotropy and exchange hardening. This reveals that there is an additional scaling-dependent factor for determining H_N; that is, the nucleation mode is affected by the scale. As the system size increases, the nucleation mode changes from a coherent rotation mode to curling or a more complicated mode.

Increasing the length reduces the internal field $\boldsymbol{H}_d$, which results in a decrease in BH above 0.5D, as depicted in Fig. 4(d). Because BH only depends on the remanent state, the value of the nucleation field itself does not affect the value of BH, apart from changing BH when the sign changes. $(BH)_{max}$ cannot occur at aspect ratios that maximize $\boldsymbol{H}_d$ (for example, at aspect ratios of $L/D = 1$, 1.6, and 4.5, where $D = 24$, 40, and 48 nm, respectively) due to the nucleation mode, as shown in Fig. 4(d).

To scale up the nanostructured exchange-coupled magnet, we assume a simple array of $n \times n$ core/shell cylinders with 2 nm intervals between the cylinders, as illustrated in Fig. 1(b). Each cylinder is free from exchange coupling. Arrays of unit cylinders with geometries of (D, t, L) = (16, 4, 144) and (24, 6, 216) are considered, with both having a positive H_N value according to Fig. 4(c). Fig. 5(a) depicts the variation in BH according to the array size n. Increasing the lateral dimension n increases BH by maximizing the internal field $\boldsymbol{H}_d$. Because the cylindrical units have the same aspect ratio but a different scale, they may be expected to demonstrate the same BH dependence on n. However, $(BH)_{max}$ is dependent on the unit geometry. With unit cylinder dimensions of (D, t, L) = (16, 4, 144), BH increases continually to 0.6554 MJ/m^3 at $n = 25$; when (D, t, L) = (24, 6, 216), BH reaches a maximum of 0.4559 MJ/m^3 at $n = 6$ and then falls rapidly as H_N becomes negative at $n > 6$ (Fig. 5(b)). This may be due to the dipole–dipole interactions among the unit cylinders in the array structure, which reduce the shape anisotropy of the unit cylinders and give rise to nonuniform cylinder-by-cylinder switching in the array structure. On the other hand, in the case of the array composed with unit cylinder of (D, t, L) = (16, 4, 144), the exchange

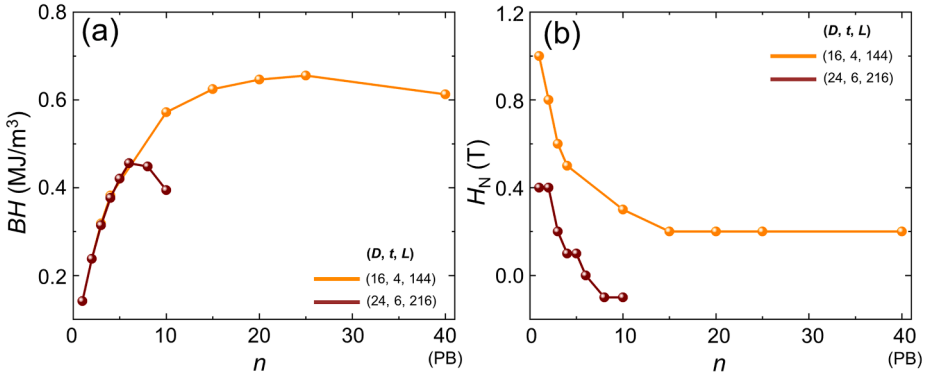

Fig. 5. (a) Energy product BH and (b) nucleation field H_N of cylindrical core/shell structure arrays as a function of n. In array structure of 40 × 40, the periodic boundary condition (PB) is applied along the × and y axes, not along the z axis.

hardening overcomes dipole–dipole interaction until $n = 40$ with periodic boundary condition, and the H_N keeps positive, which results in the *BH* follows quadratic function maximized at $\boldsymbol{H}_d = 1/2\boldsymbol{M}_s$.

Our results reveal that scaled-up bulk magnets can be fabricated through array structures of hard–soft exchange-coupled cylindrical magnets. In addition, the *BH* can be maximized by designing unit nanostructures with an optimal geometry and arranging them in an optimal array structure, with consideration of the sign of the nucleation field resulting from exchange hardening and shape anisotropy, as well as the shape anisotropy of the bulk structure due to dipole–dipole interactions among the unit structures.

4. Conclusions

We explored various geometries of cylindrical core/shell hard–soft exchange-coupled magnetic nanostructures via micromagnetic simulations to obtain a high energy product, *BH*. The scaling down of the nanostructure resulted in a high *BH* value, as a high volume-fraction of the soft-magnetic phase could be attained while maintaining a positive nucleation field by exchange hardening. We demonstrated that this nanostructured magnet could be scaled up by preparing an array of exchange-coupled cylinders. By creating needle-shaped nanostructured units and increasing the size of the array, we obtained a high *BH* value on a large scale. Our results reveal the theoretical possibility of nanostructured exchange-coupled magnets, establish guidelines for design flexibility, and demonstrate the feasibility of scalable fabrication of bulk magnets with arrays of exchange-coupled nanostructures.

CRediT authorship contribution statement

Namkyu Kim: Conceptualization, Methodology, Software, Validation, Formal analysis, Investigation, Writing - original draft, Writing - review & editing, Visualization. **Hee-Sung Han:** Methodology, Software. **Sooseok Lee:** Formal analysis. **Min-Ji Kim:** Data curation. **Dae-Han Jung:** Investigation. **Myeonghawn Kang:** Resources. **Hyejin Ok:** Resources. **Youngkyun Son:** Resources. **Sukbin Lee:** Writing - review & editing, Supervision. **Ki-Suk Lee:** Conceptualization, Methodology, Writing - original draft, Writing - review & editing, Supervision.

Declaration of Competing Interest

The authors declare that they have no known competing financial interests or personal relationships that could have appeared to influence the work reported in this paper.

Acknowledgements

This work was supported by the National Research Foundation of Korea (NRF) grant funded by the Korea government (MSIT) [Grant Nos. NRF-2019R1A2C2002996 and NRF-2016M3D1A1027831]; and by the Research Funds of Ulsan National Institute of Science and Technology (UNIST) [Nos. 1.160051.01 and 1.190038.01].

References

[1] R.W. McCallum, L. Lewis, R. Skomski, M.J. Kramer, I.E. Anderson, Annu. Rev. Mater. Res. 44 (2014) 451–477.
[2] N. Poudyal, J. Ping Liu, J. Phys. D. Appl. Phys. 46 (2013) 043301.
[3] E.F. Kneller, R. Hawig, IEEE Trans. Magn. 27 (1991) 3588–3600.
[4] R. Skomski, J.M.D. Coey, Phys. Rev. B 48 (1993) 15812–15816.
[5] E.E. Fullerton, J.S. Jiang, S.D. Bader, J. Magn. Magn. Mater. 200 (1999) 392–404.
[6] H. Zeng, J. Li, J.P. Liu, Z.L. Wang, S. Sun, Nature 420 (2002) 395–398.
[7] A.L. Wysocki, V.P. Antropov, J. Magn. Magn. Mater. 428 (2017) 274–286.
[8] Y. Shen, S.O. Leontsev, Z. Turgut, M.S. Lucas, A.O. Sheets, J.C. Horwath, IEEE Trans. Magn. 49 (2013) 3244–3247.
[9] R. Skomski, J.M.D. Coey, Scr. Mater. 112 (2016) 3–8.
[10] R. Skomski, Y. Liu, J.E. Shield, G.C. Hadjipanayis, D.J. Sellmyer, J. Appl. Phys. 107 (2010) 09A739.
[11] L. Ke, R. Skomski, T.D. Hoffmann, L. Zhou, W. Tang, D.D. Johnson, M.J. Kramer, I. E. Anderson, C.Z. Wang, Appl. Phys. Lett. 111 (2017), 022403.
[12] A. Chakraborty, R. Hirian, G. Kapun, V. Pop, Nanomaterials 10 (2020) 1308.
[13] J. Lee, J. Kim, D. Kim, G. Lee, Y.-B. Oh, T.-Y. Hwang, J. Lim, H. Cho, J. Kim, Y. Choa, ACS Appl. Mater. Interfaces 11 (2019) 26222–26227.
[14] H. Ryo, L. Hu, J. Kim, Y. Yang, IEEE Trans. Magn. 53 (2017) 7400207.
[15] W. Schärtl, Nanoscale 2 (2010) 829–843.
[16] S.A. Sebt, A. Bakhshayeshi, M.R. Abolhassani, J. Stat. Mech. Theory Exp. (2012) P09006.
[17] H. Fukunaga, R. Horikawa, M. Nakano, T. Yanai, T. Fukuzaki, K. Abe, IEEE Trans. Magn. 49 (2013) 3240–3243.
[18] R.G. Chaudhuri, S. Paria, Chem. Rev. 112 (2012) 2373–2433.
[19] A. López-ortega, M. Estrader, G. Salazar-alvarez, A.G. Roca, J. Nogues, Phys. Rep. 553 (2015) 1–32.
[20] J.S. Jiang, J. Appl. Phys. 117 (2015) 17A734.
[21] J. Zou, L. Shen, L. Qiu, Y. Feng, C. Luo, X. Liang, L. Zhao, G. Zhao, J. Rare Earths 37 (2019) 1034–1039.
[22] L. Qiu, L. Zhao, X. Weng, L. Shen, G. Zhao, F. Wang, L. Xie, J. Rare Earths 37 (2019) 1030–1033.
[23] Y. Xiang, C.W. Chen, J. Magn. Magn. Mater. 430 (2017) 1–5.
[24] V.L. Kurichenko, D.Y. Karpenkov, P.A. Gostischev, J. Phys. Condens. Matter 32 (2020).
[25] P.-O. Jubert, IEEE Trans. Magn. 50 (2014) 3002004.
[26] J.S. Jiang, S.D. Bader, J. Phys. Condens. Matter 26 (2014), 064214.
[27] A. Vansteenkiste, J. Leliaert, M. Dvornik, M. Helsen, F. Garcia-Sanchez, B. Van Waeyenberge, AIP Adv. 4 (2014), 107133.
[28] J.P. Liu, E. Fullerton, O. Gutfleisch, D.J. Sellmyer, Nanoscale Magnetic Mateirals and Applications, Springer, US, 2009.
[29] Yi Liu, David J. Sellmyer, Daisuke Shindo (Eds.), Handbook of Advanced Magnetic Materials, Springer US, Boston, MA, 2006.
[30] G.C. Hadjipanayis, G.A. Prinz, A. Gary, Science and Technology of Nanostructured Magnetic Materials, Springer, US, 2013.
[31] P. Toson, A. Asali, W. Wallisch, G. Zickler, J. Fidler, IEEE Trans. Magn. 51 (2015) 7400104.
[32] E. Anagnostopoulou, B. Grindi, L. Lacroix, F. Ott, I. Panagiotopoulos, G. Viau, Nanoscale 8 (2016) 4020–4029.
[33] J.M.D. Coey, Magnetism and Magnetic Materials, Cambridge University Press, Cambridge, 2010.